Electronic Supporting Information (ESI) for the paper:

An experimental and theoretical investigation of the N(^{2}D) + C$_6$H$_6$ (benzene) reaction with implications for the photochemical models of Titan

Nadia Balucani,[*][a] Adriana Caracciolo,[a‡] Gianmarco Vanuzzo,[a] Dimitrios Skouteris,[b] Marzio Rosi,[c] Leonardo Pacifici,[a] Piergiorgio Casavecchia,[a] Kevin M. Hickson,[*d] Jean-Christophe Loison,[d] and Michel Dobrijevic[e]

^{a} *Dipartimento di Chimica, Biologia e Biotecnologie, Università degli Studi di Perugia, 06123 Perugia, Italy*
E-mail: nadia.balucani@unipg.it
^{b} *Master-Tec SrL, Via Sicilia, 41, 06128 Perugia, Italy*
^{c} *Dipartimento di Ingegneria Civile e Ambientale, Università degli Studi di Perugia, 06100, Perugia, Italy*
^{d} *Univ. Bordeaux, CNRS, Bordeaux INP, ISM, UMR 5255, F-33400 Talence, France*
^{e} *Univ. Bordeaux, CNRS, LAB, UMR 5804, F-33600 Pessac, France*

‡*Present address: Institute of Chemistry and Chemical Engineering, École Polytechnique Fédérale de Lausanne, 1015 Lausanne, Switzerland*

Table of Contents

1. Experimental Details

1.1 Crossed Molecular Beam Experiments

1.1.1 Beam conditions

The study of the title reaction has been possible following the development in our laboratory of a continuous supersonic beam of nitrogen atoms containing, in addition to the electronic ground state ^{4}S, a sizeable amount of the excited, metastable state ^{2}D. This has been achieved via a high-pressure radio-frequency (RF) discharge beam source described in Ref. 1. The atomic nitrogen beam used in this experiment was produced by discharging 90 mbar of a 2.5% N_2/He gas mixture through a water-cooled 0.48 mm diameter quartz nozzle at 250 W of RF power. The beam was collimated by a 0.8 mm diameter boron nitride skimmer and a further defining aperture to an angular divergence of 2.4°. High molecular dissociation (about 60%) was achieved. Atomic nitrogen was produced in a distribution of electronic states which has been characterized in our laboratory by Stern-Gerlach magnetic analysis: 72% of N atoms are in the ^{4}S ground state, while 21% and 7% are in the metastable excited states ^{2}D and ^{2}P states, respectively.[1] The resulting beam peak velocity and speed ratio were 2253 m/s and 4.6, respectively. In our previous experiments on N(^{2}D) reactions,[2-16] we verified that the presence of N(^{4}S) and N(^{2}P) in the nitrogen beam did not affect the experimental outcomes as there are no features in the scattering distributions that can be associated to their reactions. Indeed, the rate constants of N(^{4}S) and N(^{2}P) reactions with several hydrocarbons are known to be much smaller with respect to those of N(^{2}D) and/or non-reactive.[17-19] This seems to be the same also for the title reaction as no clue of more energetic products from the N(^{2}P) reactions are present in the scattering distributions. Notably, a recent experiment on the reaction of N(^{2}P) with toluene ions suggests that at least the reactions with charged species can be efficient for the ^{2}P state of atomic nitrogen.[20]

The supersonic beam of benzene was generated by expanding 103 mbar of neat gas (99.8% purity) through a 0.1 mm diameter stainless-steel nozzle, followed by a 0.8 mm skimmer and a further defining aperture (beam angular divergence 3.8°). The benzene pressure was kept constant by maintaining a sample of liquid benzene at 17° C (the Pyrex flask containing liquid benzene was immersed in a water/ethylene glycol bath). The peak velocity of benzene was measured to be 521 m/s with a speed ratio of 4.2.

1.1.2 Time-of-flight spectrum at m/z=91 and m/z=65 recorded at Θ=48°

The presence of two different contributions to the signal recorded at $m/z = 65$ is clearly visible also in the TOF spectra. Fig. S1 compares the TOF spectra at $m/z = 91$ (top panel) and $m/z = 65$ (bottom panel) at Θ=48° and relates them to the Newton diagram (note that the Newton diagram is represented in the velocity space while the TOF distributions are recorded in the time space). As can be seen, the TOF spectrum recorded at $m/z = 91$ ($C_6H_5N^+$) at the LAB angle Θ = 48° (close to the CM angle) is characterized by a slow peak centered at about 380 μs, which corresponds to nearly the velocity of the center-of-mass of the system and is attributed to the heavy co-product(s) of gross formula C_6H_5N in the H-displacement channels. The similar peak observed at $m/z = 65$ is attributed to the same C_6H_5N products detected at the - 26 daughter ion $C_5H_5^+$. A much faster peak at about 160 μs is also visible and this clearly corresponds to a completely different reaction product from another channel which, on the basis of energy and momentum conservation, can only be attributed to the cyclopentadienyl radical from the reaction channel (1) and/or (2) (C_5H_5 + HNC and/or C_5H_5 + HNC), with a possible contribution also from the channels (4) and (5). Unfortunately, on the basis of the product translational

energy distribution used to fit the LAB angular and TOF distributions at $m/z = 65$ alone it is not possible to quantify the relative importance of the (1), (2), (4) and (5) channels.
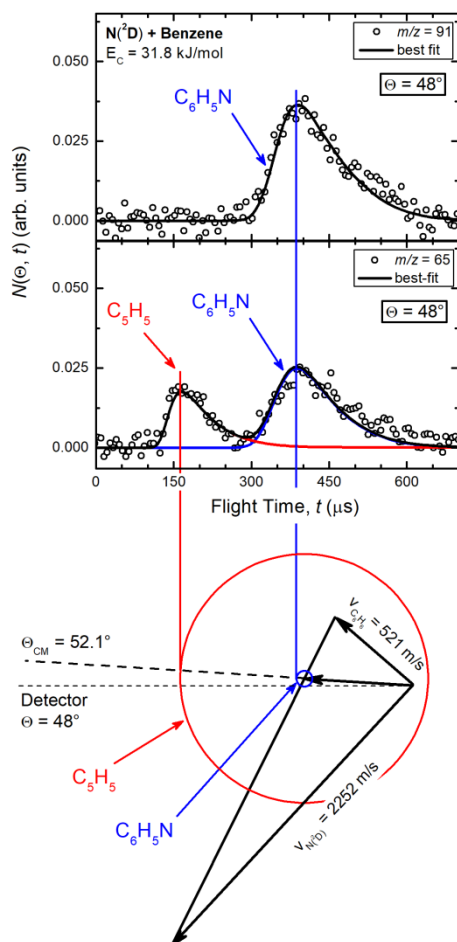

Fig. S1 $m/z = 91$ (top panel) and $m/z = 65$ (bottom panel) TOF distribution recorded at $\Theta = 48°$. The black solid curves superimposed on the experimental data (dots) are the simulated TOF distributions obtained by using the best-fit CM functions shown in Fig. 4. In this case, the radius of each circle in the Newton diagram has been drawn considering the peak of the best-fit translational energy distributions).

1.2 Kinetic Experiments

1.2.1 N(²D) production

The photolytic production of N(^{2}D) is not trivial, so these atoms were produced chemically during the present study, employing reaction (11) as a source as previously characterized by Nuñez-Reyes *et al.*[21]

$$C(^3P) + NO \rightarrow N(^2D, ^4S) + CO \tag{11}$$
$$C(^3P) + NO \rightarrow O(^3P) + CN \tag{12}$$

The [N(^{2}D)+N(^{4}S)]/[O(^{3}P)]) branching ratio has been estimated as 1.5±0.3 at room temperature.[22] C(^{3}P) atoms were produced by the 266 nm pulsed laser photolysis of CBr$_4$, introduced into the supersonic flow upstream of the Laval nozzle in trace quantities ($<4\times10^{13}$ cm^{-3}). For this purpose, solid CBr$_4$ was held in a flask at a known pressure and temperature while a fraction of the carrier gas

flow was diverted through it (<70 sccm) before rejoining the main flow. Pulse energies lower than 40 mJ (10 Hz, 5 mm beam diameter) were employed here. Previous work has shown that excited state $C(^1D)$ atoms are also produced by CBr_4 photolysis under similar conditions to the present experiments at the level of 10-15 %.[23] $C(^1D)$ atoms react rapidly with NO,[24] and are expected to lead to the same products of (11) and (12). NO concentrations were kept at a constant value for each series of experiments at a specific temperature with values in the range $(3.0-6.4) \times 10^{14}$ cm^{-3}. In contrast to $N(^2D)$ atoms, $C(^1D)$ atoms are rapidly quenched by collisions with N_2,[25] whereas quenching with Ar is slow,[26] so the influence of $C(^1D)$ reactions on $N(^2D)$ kinetics can be verified by performing experiments at the same temperature with both of these carrier gases. Such experiments were performed at room temperature during our recent studies of the $N(^2D)$ + allene reaction,[13] with essentially identical rate constants obtained for both carrier gases.

1.2.2 N(²D) detection

The $N(^2D)$ atom kinetics were followed by pulsed laser induced fluorescence in the vacuum ultraviolet wavelength range (VUV LIF) at 116.745 nm via the $2s^2 2p^3$ $^2D° - 2s^2 2p^3 (^3P)3d$ ^2F electronic transition. Tunable narrowband radiation at this wavelength was generated by first frequency doubling the output of a 10 Hz pulsed dye laser at 700.5 nm in a beta barium borate crystal. The residual dye laser radiation was separated from the UV beam at 350.2 nm (8-9 mJ per pulse) by two dichroic mirrors with peak reflectivity at 355 nm before being steered and focused into a frequency tripling cell attached to the reactor containing a mixture of Xe (40 Torr), with Ar added (560 Torr) for phase matching. The resulting tunable VUV beam was collimated by a MgF_2 lens at the exit of the cell, which also served to steer it along a 75 cm long sidearm containing circular baffles and into the reactor where it crossed the supersonic flow at the level of the observation axis. This region was continuously flushed by N_2 or Ar to minimize absorption of the VUV beam by reactive gases in the chamber. As the residual UV light was divergent after exiting the MgF_2 lens, due to the difference in MgF_2 refractive index between UV and VUV wavelengths, it was mostly blocked by the circular baffles. A fraction of the fluorescence emitted by unreacted $N(^2D)$ atoms within the reactor was collected at right angles to the flow and the probe laser beam by a lithium fluoride (LiF) lens which focused the VUV emission onto the photocathode of a solar blind photomultiplier tube (PMT). The sensitive envelope of the PMT and the LiF lens were protected from reactive gases within the chamber by a LiF window, while the zone between the LiF window and the PMT was evacuated by a dry pump to prevent further emission losses by atmospheric O_2 absorption. The signal output of the PMT was processed by a boxcar integrator interfaced to a personal computer for display and averaging purposes. As the CBr_4 molecules within the reactor scattered some of the photolysis laser light causing saturation of the PMT, all data recorded during the first five microseconds following the photolysis pulse were unexploitable. Approximately 100 time points were recorded to establish each kinetic profile, with time points consisting of the average signal of 30 individual laser shots. Fifteen of these time points occurred at negative time delays, that is, with the probe laser firing prior to the photolysis laser pulse to determine the baseline level.

1.2.3 Flow conditions and C₆H₆ concentration determination

Co-reagent C_6H_6 was carried into the reactor by bubbling a small fraction of the carrier gas flow (<30 sccm) through a vessel containing C_6H_6 at room temperature and a known pressure. The C_6H_6

laden gas was flowed into a cold trap maintained at 290 K to ensure that the amount of C_6H_6 vapour exiting the trap corresponded to its saturated vapour pressure value at 290 K.[27] The exit of the cold trap was connected to the Laval nozzle reservoir via a heating hose maintained at 353 K. Upon entering the Laval nozzle reservoir, the C_6H_6 vapour was further diluted by the main carrier gas flow, so we assume that no further condensation losses occurred upstream of the cold trap. The carrier gas flows into the CBr_4 vessel, the C_6H_6 flask and the main flow into the reactor as well as the NO flow into the reactor were all controlled by calibrated mass-flow controllers allowing the co-reagent NO and C_6H_6 concentrations to be calculated precisely. The gases themselves (Messer Ar 99.999%, N_2 99.995%, Linde Xe 99.999%, Air Liquide NO 99.9%) were flowed directly from the cylinders without further purification.
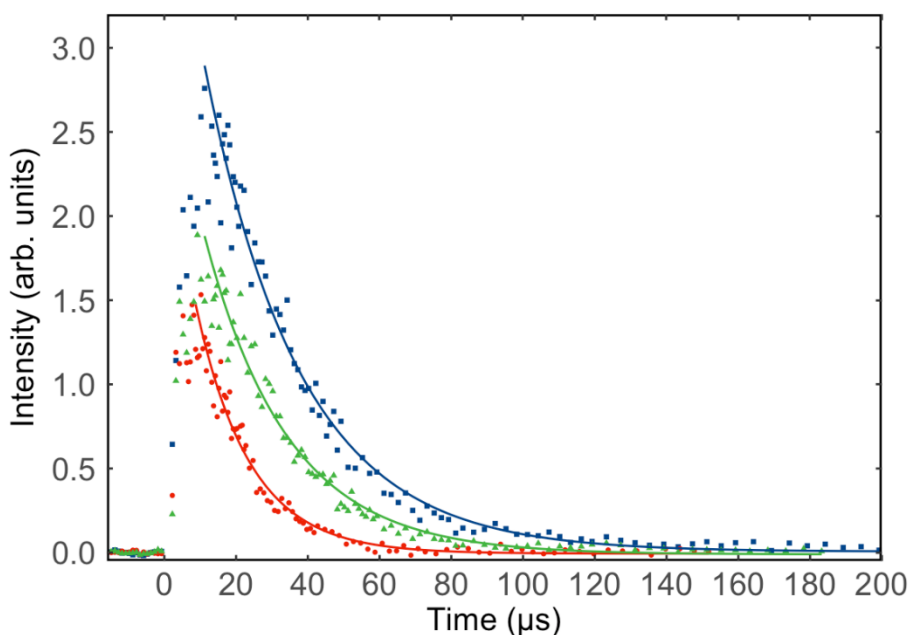

Fig. S2 $N(^2D)$ fluorescence signal, recorded at 127 K, plotted as a function of reaction time. (Solid blue squares) without C_6H_6; (solid green triangles) $[C_6H_6] = 3.6 \times 10^{13}$ cm^{-3}; (solid red circles) $[C_6H_6]$ $= 1.7 \times 10^{14}$ cm^{-3}. $[NO] = 4.6 \times 10^{14}$ cm^{-3} for all traces. Solid lines represent exponential fits to the data using expression (16).

Table S1 Second-order rate constants for the $N(^2D) + C_6H_6$ reaction alongside other relevant information.

T / K	N^b	$[C_6H_6]$ / 10^{14} cm^{-3}	$[NO]/10^{14} cm^{-3}$	$k_{N(^2D)+C_6H_6}/10^{-11}$ cm^3s^{-1}
296	30	0 – 2.1	6.4	(23.4 ± 2.5)
177 ± 2^a	33	0 – 1.4	4.1	(18.1 ± 2.0)
127 ± 2	33	0 – 1.7	4.6	(20.5 ± 2.4)
75 ± 2	30	0 – 0.7	3.0	(21.9 ± 2.4)
50 ± 1	18	0 – 0.8	4.2	(25.5 ± 4.5)

[a]Uncertainties on the temperatures represent the statistical (1σ) errors obtained from Pitot tube measurements of the impact pressure. [b]Number of individual measurements. [c]Uncertainties on the measured rate constants represent the combined statistical (1σ) and estimated systematic (10%) errors.

2. Computational results

2.1 Enthalpy changes and barrier heights

Table S2. Enthalpy changes and barrier heights (kJ/mol, 0 K) computed at the CCSD(T)/aug-cc-pVTZ + ZPE (CBS + ZPE) levels of theory for selected dissociation and isomerization processes for the system $N(^2D) + C_6H_6$.

	ΔH^0_0	Barrier height
$N(^2D) + C_6H_6 \rightarrow$ **i1**	-183 (-218)	
i1 $\rightarrow$ **i2**	-127 (-108)	1 (12)
i2 $\rightarrow$ **i3**	51	187
i3 $\rightarrow$ **P12 (C_6H_5N + H)**	163	184
i3 $\rightarrow$ **i4**	-245	20
i1 $\rightarrow$ **i4**	-321 (-312)	45 (53)
i4 $\rightarrow$ **P13 (C_6H_5 + NH)**	425	
i4 $\rightarrow$ **P1 (C_6H_5N + H)**	363 (373)	
i4 $\rightarrow$ **i10**	93	263
i10 $\rightarrow$ **P4 (C_6H_4 + NH_2)**	285	
i4 $\rightarrow$ **i19**	114 (115)	289 (288)
i1 $\rightarrow$ **i19**	-207	63
i19 $\rightarrow$ **P1 C_6H_5N + H)**	249 (233)	
i19 $\rightarrow$ **i20**	-10 (-6)	78 (76)
i20 $\rightarrow$ **P14 (C_6H_5N + H)**	311	
i20 $\rightarrow$ **i21**	-51 (-53)	136 (139)
i21 $\rightarrow$ **i16**	81 (89)	242 (241)
i16 $\rightarrow$ **P9 (C_5H_5 + HCN)**	-4 (-12)	57 (53)
i16 $\rightarrow$ **P2 (C_5H_5CN + H)**	101	125
i21 $\rightarrow$ **P10 (C_5H_6 + CN)**	260	
i21 $\rightarrow$ **P2 (C_5H_5CN + H)**	182	194
i21 $\rightarrow$ **P11 (C_5H_5CN + H)**	156 (163)	180 (179)
i4 $\rightarrow$ **i5**	196	231
i5 $\rightarrow$ **i6**	-10	70
i6 $\rightarrow$ **i16**	-52	128

i6 → i11	-105	138
i11 → P6 (C₅H₄ + HCNHcis)	460	
HCNHcis → HCNHtrans	-11	41
i6 → P2 (C₅H₅CN + H)	49	84
i6 → P5 (C₅H₅ + HNC)	3	59
HNC → HCN	-60 (-60)	124
i2 → i12	-108 (-113)	26 (20)
i12 → i15	80 (83)	184 (182)
i15 → i18	43	111
i18→ P9 (C₅H₅ + HCN)	-79	51
i15 → i16	-32 (-29)	54 (51)
i2 → i7	37	68
i7 → i8	47	95
i8 → i9	-44	113
i9 → i17	152	218
i17 → i18	-177	21
i9 → P3 (C₅H₅N + CH)	225	
i12 → P16 (C₆H₅N + H)	324 (329)	
i12 → P17 (C₆H₅N + H)	445	
i12 → P15 (C₆H₅N + H)	303 (307)	
i12 → i13	125 (125)	208 (205)
i13 → i14	-22 (-22)	87 (84)
i14 → i22	-14 (-14)	176 (179)
i22 → P8 (C₄H₄NCCH + H)	179 (178)	187 (186)
i14 → P8 (C₄H₄NCCH + H)	165 164)	187 (186)
i14 → P7 (C₄H₄N + C₂H₂)	69 (67)	158 (154)
i13 → P18 (C₄H₃NC₂H₂ + H)	214	

i6 → i11	-105	138
i11 → P6 (C_5H_4 + HCNHcis)	460	
HCNHcis → HCNHtrans	-11	41
i6 → P2 (C_5H_5CN + H)	49	84
i6 → P5 (C_5H_5 + HNC)	3	59
HNC → HCN	-60 (-60)	124
i2 → i12	-108 (-113)	26 (20)
i12 → i15	80 (83)	184 (182)
i15 → i18	43	111
i18→ P9 (C_5H_5 + HCN)	-79	51
i15 → i16	-32 (-29)	54 (51)
i2 → i7	37	68
i7 → i8	47	95
i8 → i9	-44	113
i9 → i17	152	218
i17 → i18	-177	21
i9 → P3 (C_5H_5N + CH)	225	
i12 → P16 (C_6H_5N + H)	324 (329)	
i12 → P17 (C_6H_5N + H)	445	
i12 → P15 (C_6H_5N + H)	303 (307)	
i12 → i13	125 (125)	208 (205)
i13 → i14	-22 (-22)	87 (84)
i14 → i22	-14 (-14)	176 (179)
i22 → P8 (C_4H_4NCCH + H)	179 (178)	187 (186)
i14 → P8 (C_4H_4NCCH + H)	165 164)	187 (186)
i14 → P7 (C_4H_4N + C_2H_2)	69 (67)	158 (154)
i13 → P18 ($C_4H_3NC_2H_2$ + H)	214	

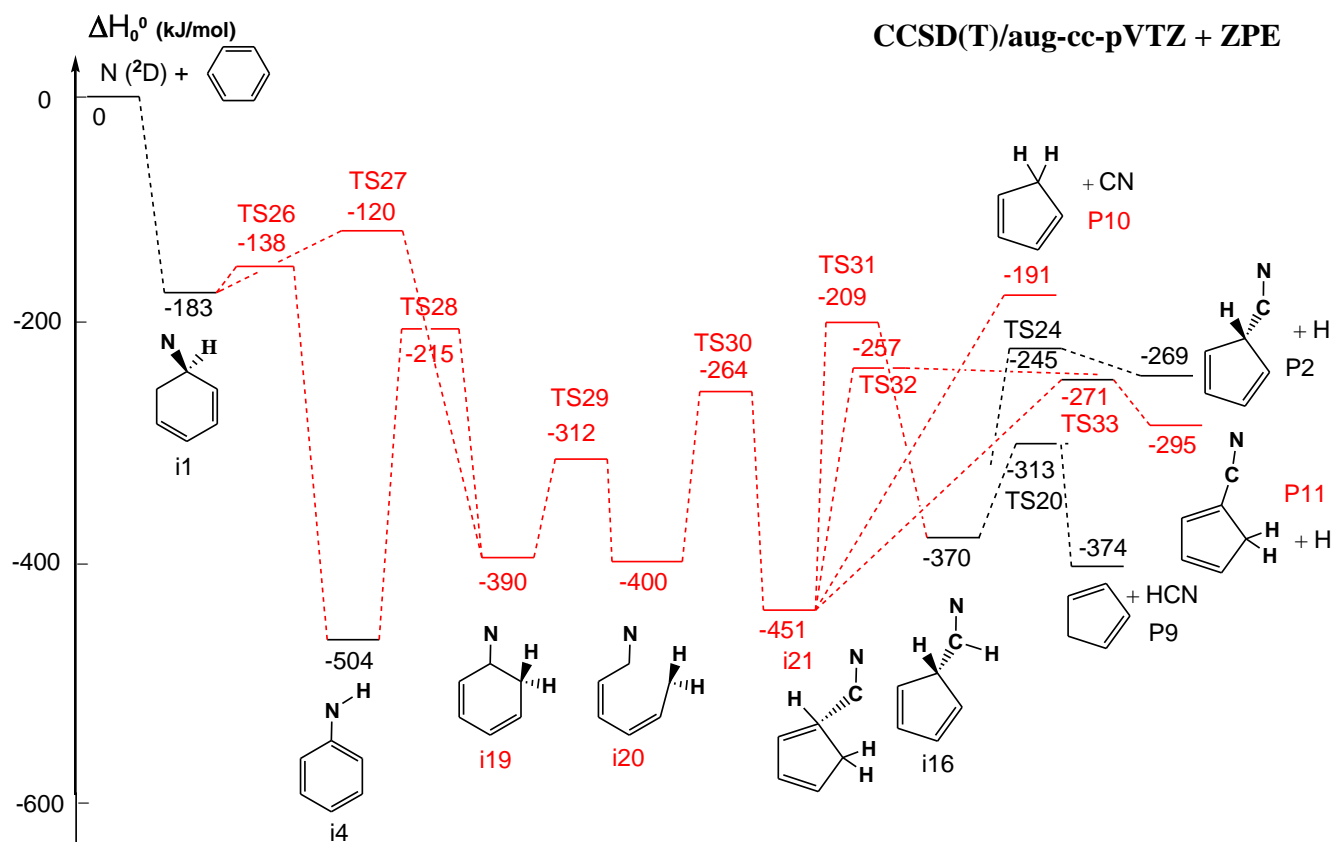## 2.2 Less favoured pathways in the potential energy surface

Figure S3: PES for the reaction between N(^{2}D) and benzene, leading to the formation of C_5H_5 + HCN (P9), C_5H_5CN + H (P11), C_5H_5CN + H (P2), C_5H_6 + CN (P10). Relative energies computed at CCSD(T)/aug-cc-pVTZ//B3LYP/aug-cc-pVTZ level[28-35] in kJ/mol. The red paths were not calculated in the work of Chin et al.[36]
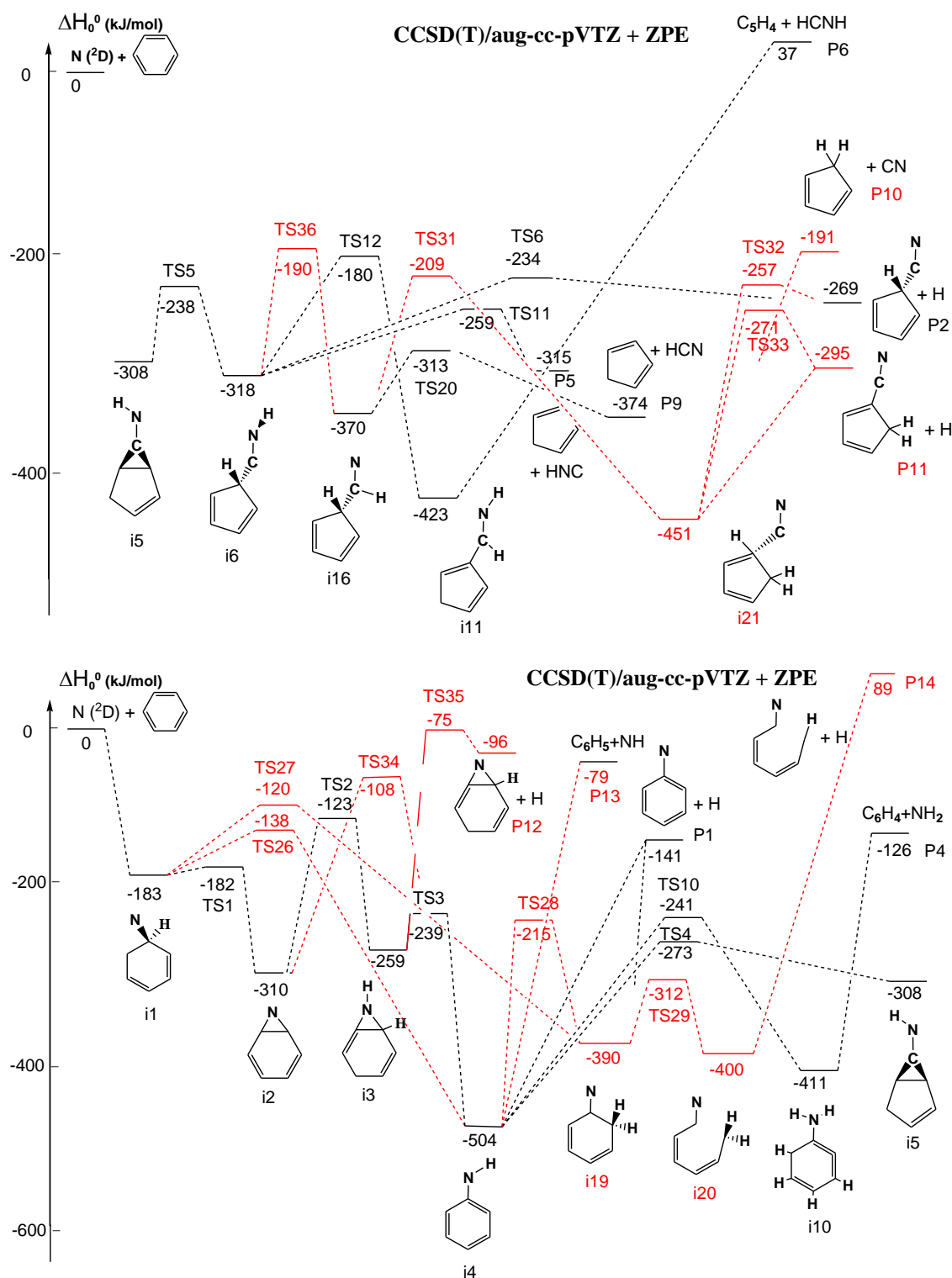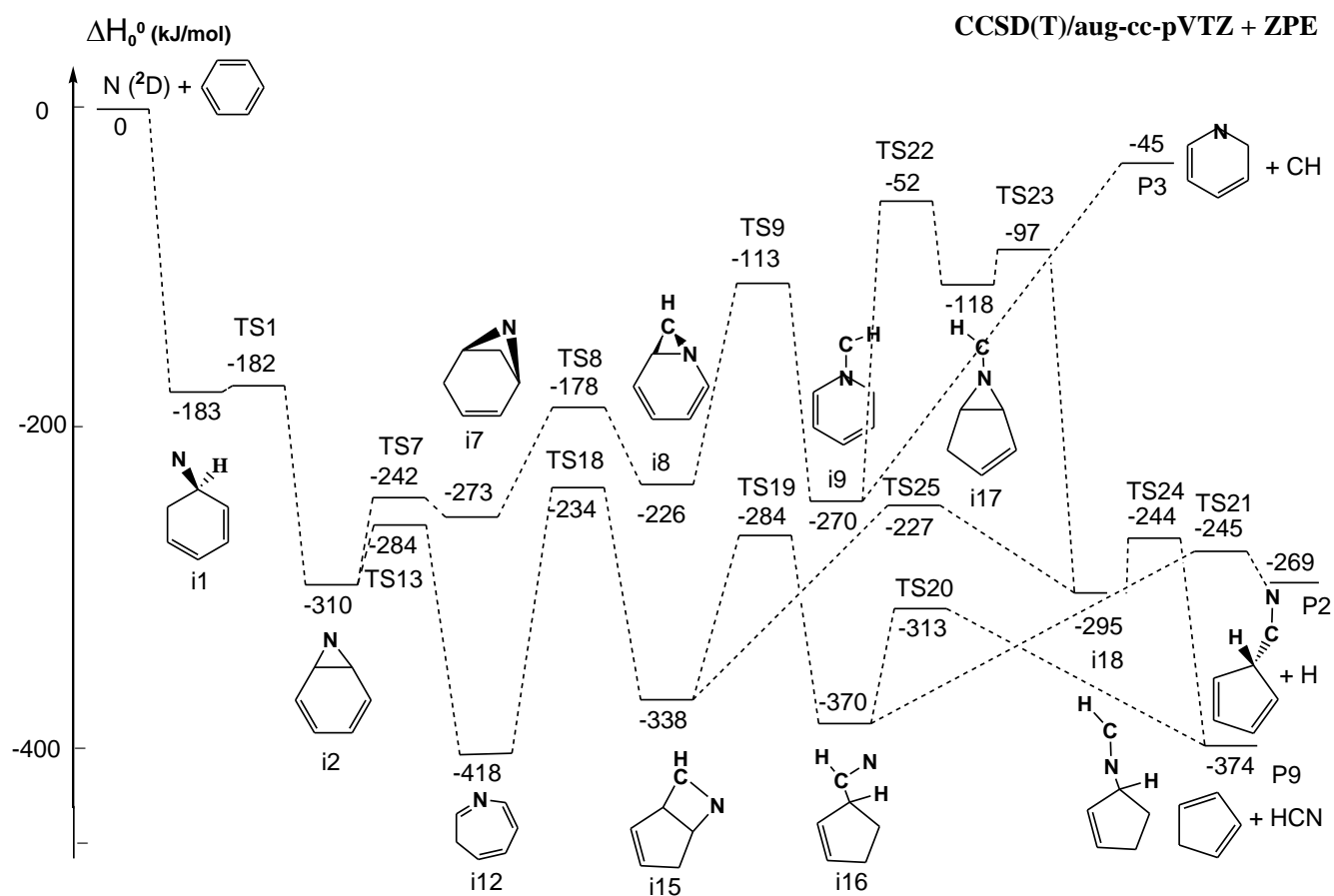
Figure S4: PES for the reaction between N(^{2}D) and benzene, leading to the formation of C_6H_5N + H (P1), C_6H_4 + NH_2 (P4), C_6H_5 + NH (P13), C_6H_5N + H (P12), C_6H_5N + H (P14) (lower panel) and C_5H_5 + HCN (P9), C_5H_5 + HNC (P5), C_5H_5CN + H (P11), C_5H_5CN + H (P2), C_5H_6 + CN (P10), C_5H_4 + HCNH (P6) (upper panel). The upper panel shows the reactivity of minimum i5. Relative energies computed at CCSD(T)/aug-cc-pVTZ//B3LYP/aug-cc-pVTZ level[28-35] in kJ/mol. The red paths were not calculated in the work of Chin et al.[36]

Figure S5: PES for the reaction between N(^{2}D) and benzene, leading to the formation of C_5H_5 + HCN (P9), C_5H_5CN + H (P2) and C_5H_5N + CH (P3). Relative energies computed at CCSD(T)/aug-cc-pVTZ//B3LYP/aug-cc-pVTZ level[28-35] in kJ/mol.
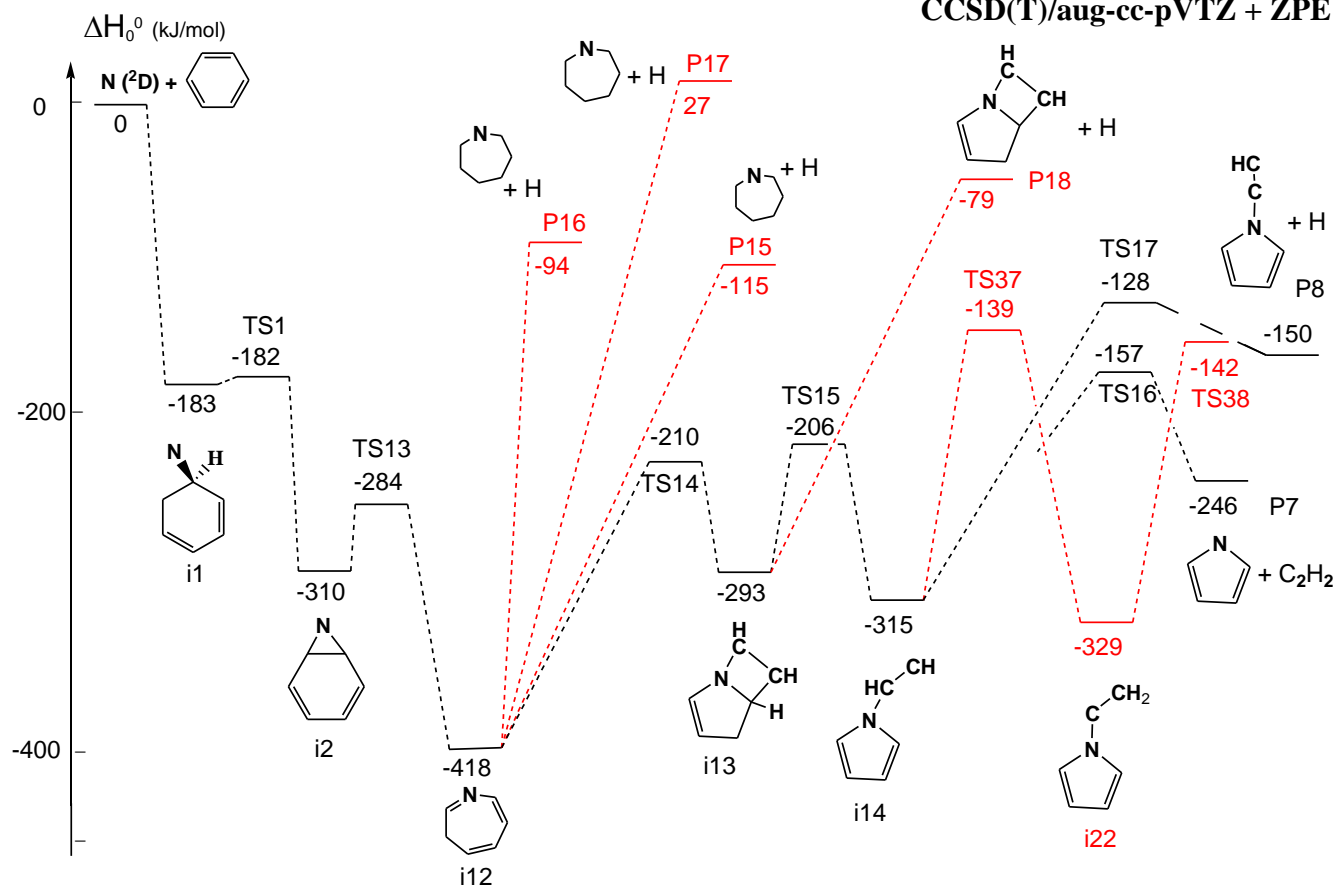
Figure S6: PES for the reaction between $N(^2D)$ and benzene, leading to the formation of C_4H_4N + C_2H2 (P7), C_4H_4NCCH + H (P8), C_6H_5N + H (P15), C_6H_5N + H (P16), C_6H_5N + H (P17), C_4H_3NCHCH + H (P18). Relative energies computed at CCSD(T)/aug-cc-pVTZ//B3LYP/aug-cc-pVTZ level[28-35] in kJ/mol. The red paths were not calculated in the work of Chin et al.[36]

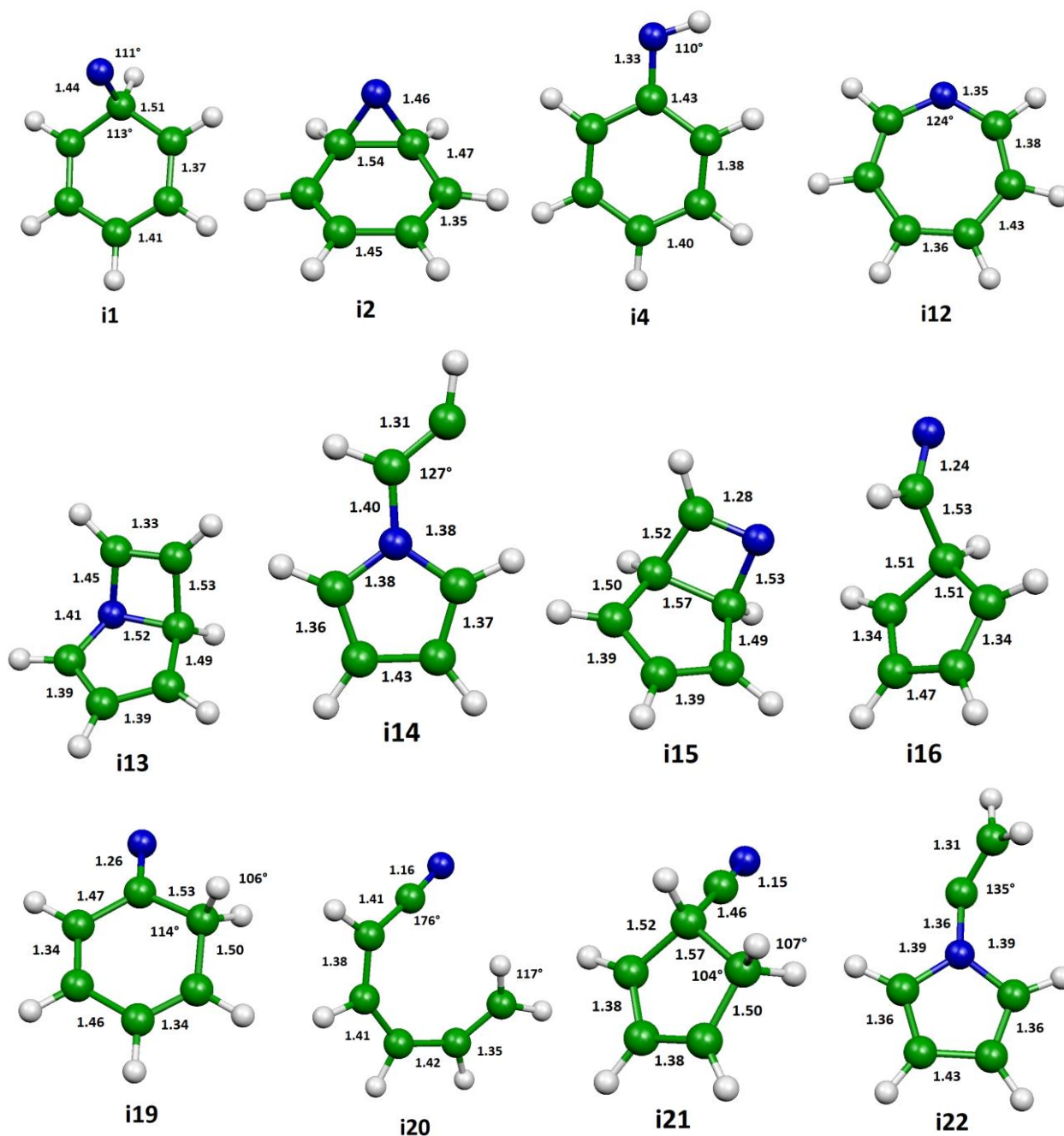## 2.3 Structure of the main intermediates, products and transition states.

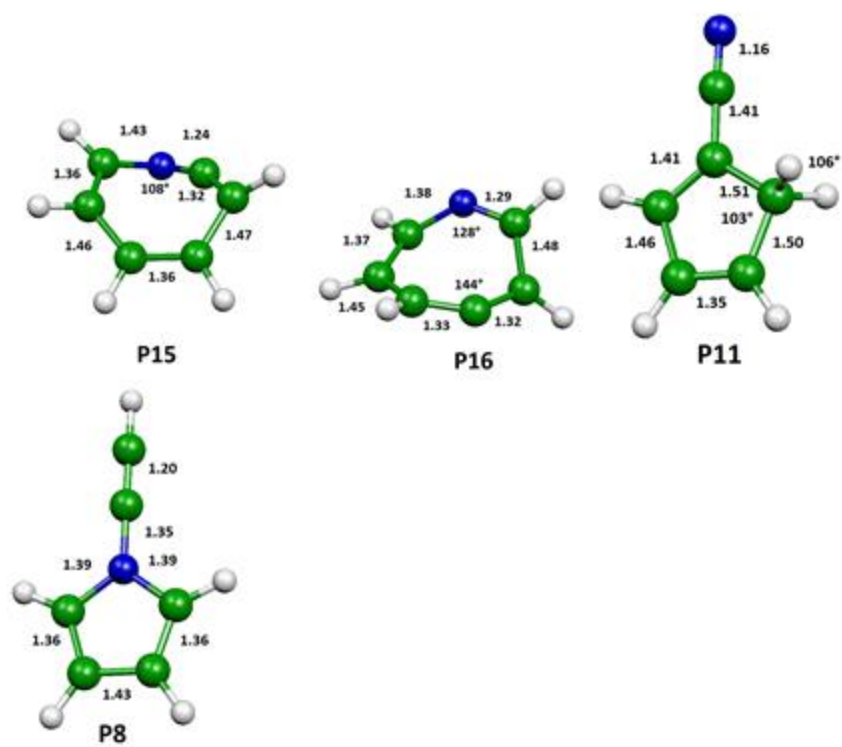**Figure S7:** The structure of the main intermediates along the PES.

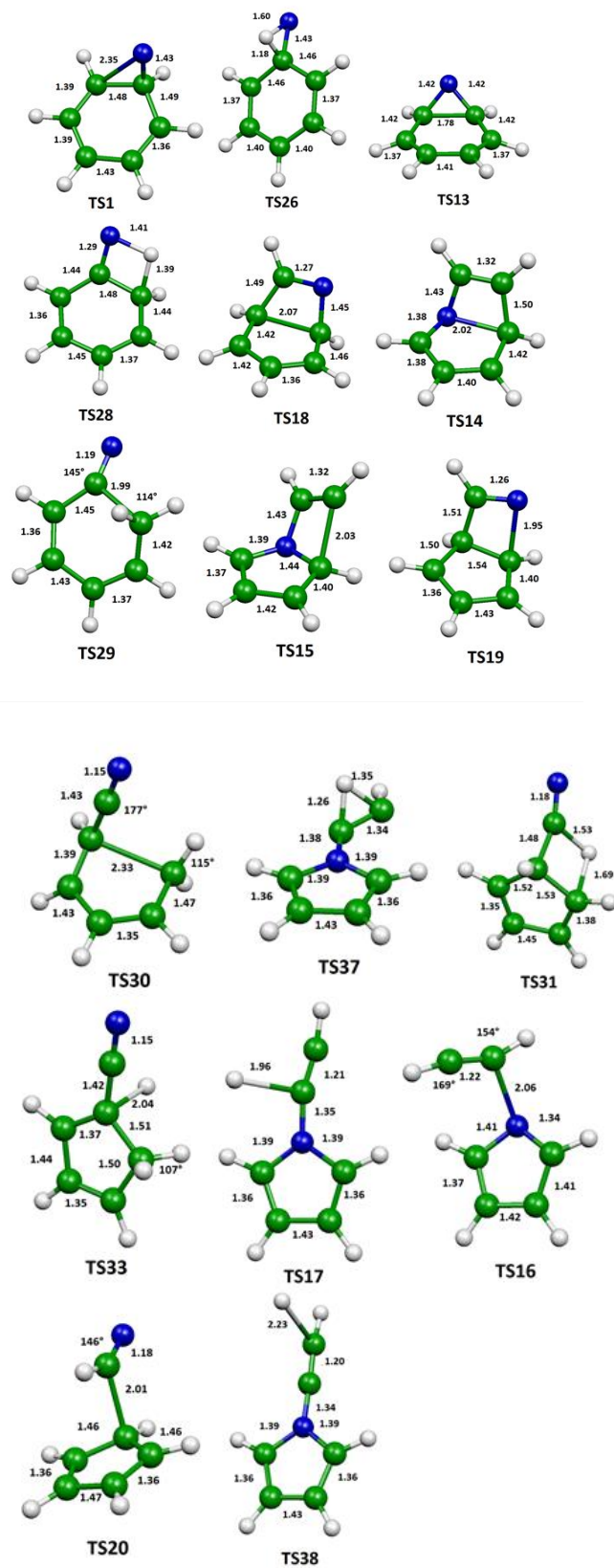**Figure S8:** The structure of several products.

Figure S9: The structure of the most important transition states along the PES.

References

1. M. Alagia, V. Aquilanti, D. Ascenzi, N. Balucani, D. Cappelletti, L. Cartechini, P. Casavecchia, F. Pirani, G. Sanchini and G. G. Volpi, *Israel J. Chem.*, 1997, 37, 329–342.

2. N. Balucani, A. Bergeat, L. Cartechini, G. G. Volpi, P. Casavecchia, D. Skouteris and M. Rosi, *J. Phys. Chem. A*, 2009, 113, 11138–11152.

3. N. Balucani, P. Casavecchia, L. Bañares, F. J. Aoiz, T. Gonzales-Lezana, P. Honvault and J. M. Launay, *J. Phys. Chem. A* 2006, 110, 817–829.

4. N. Balucani, M. Alagia, L. Cartechini, P. Casavecchia, G. G. Volpi, L. A. Pederson and G. C. Schatz, *J. Phys. Chem. A*, 2001, 105, 2414–2422.

5. N. Balucani, L. Cartechini, G. Capozza, E. Segoloni, P. Casavecchia, G. G. Volpi, L. Bañares, F. J. Aoiz, P. Honvault and J.-M. Launay, *Phys. Rev. Lett.*, 2002, 89, 013201-1-013201-4.

6. Z. Homayoon, J. M. Bowman, N. Balucani and P. Casavecchia, *J. Phys. Chem. Lett.*, 2014, 5, 3508–3513.

7. N. Balucani, L. Cartechini, P. Casavecchia, Z. Homayoon and J. M. Bowman, *Mol. Phys.*, 2015, 113, 2296–2301.

8. N. Balucani, F. Leonori, R. Petrucci, M. Stazi, D. Skouteris, M. Rosi and P. Casavecchia, *Faraday Discuss.*, 2010, 147, 189–216.

9. N. Balucani, M. Alagia, L. Cartechini, P. Casavecchia, G. G. Volpi, K. Sato, T. Takayanagi and Y. Kurosaki, *J. Am. Chem. Soc.*, 2000, 122, 4443–4450.

10. N. Balucani, L. Cartechini, M. Alagia, P. Casavecchia and G. G. Volpi, *J. Phys. Chem. A* 2000, 104, 5655–5659.

11. N. Balucani, D. Skouteris, F. Leonori, R. Petrucci, M. Hamberg, W. D. Geppert, P. Casavecchia and M. Rosi, *J. Phys. Chem. A*, 2012, 116, 10467–10479.

12. L. Mancini, G. Vanuzzo, D. Marchione, G. Pannacci, P. Liang, P. Recio, M. Rosi, D. Skouteris, P. Casavecchia and N. Balucani, *J. Phys. Chem. A*, 2021, 125, 8846–8859.

13. G. Vanuzzo, L. Mancini, G. Pannacci, P. Liang, D. Marchione, P. Recio, Y. Tan, M. Rosi, D. Skouteris, P. Casavecchia, N. Balucani, K. M. Hickson, J.-C. Loison and M. Dobrijevic, *ACS Earth Space Chem.*, 2022, 6, 2305–2321.

14. P. Liang, L. Mancini, D. Marchione, G. Vanuzzo, F. Ferlin, P. Recio, Y. Tan, G. Pannacci, L. Vaccaro, M. Rosi, P. Casavecchia and N. Balucani, *Mol. Phys.*, 2022, 120, e1948126.

15. G. Vanuzzo, D. Marchione, L. Mancini, P. Liang, G. Pannacci, P. Recio, Y. Tan, M. Rosi, D. Skouteris, P. Casavecchia and N. Balucani, *J. Phys. Chem. A*, 2022, 126, 6110– 6123.

16. P. Recio, D. Marchione, A. Caracciolo, V. J. Murray, L. Mancini, M. Rosi, P. Casavecchia and N. Balucani, *Chem. Phys. Lett.*, 2021, **779**, 138852.

17. O. Dutuit, *et al.*, *Astrophys. J. Suppl. Ser.*, 2013, **204**, 20 (45pp).

18. K. Sato, K. Misawa, Y. Kobayashi, M. Matsui, S. Tsunashima, Y. Kurosaki and T. Takayanagi, *J. Phys. Chem. A*, 1999, **103**, 8650–8656.

19. T. Suzuki, Y. Shihira, T. Sato, H. Umemoto and S. Tsunashima, *J. Chem. Soc. Faraday Trans.*, 1993, **89**, 995–999.

20. A. I. Begley, N. S. Shuman, B. A. Long, R. Kämpf, L. Gyr, A. A. Viggiano and R. Zenobi, *J. Phys. Chem. A*, 2022, **126**, 1743−1754

21. D. Nuñez-Reyes and K. M. Hickson, *Phys. Chem. Chem. Phys.*, 2018, **20**, 17442–17447.

22. A. Bergeat, T. Calvo, G. Dorthe and J.-C. Loison, *Chem. Phys. Lett.* 1999, **308**, 7-12.

23. R. J. Shannon, C. Cossou, J.-C. Loison, P. Caubet, N. Balucani, P. W. Seakins, V. Wakelam and K. M. Hickson, *RSC Adv.*, 2014, **4**, 26342–26353.

24. D. Nuñez-Reyes and K. M. Hickson, *Chem. Phys. Lett.* 2017, **687**, 330-335.

25. K. M. Hickson, J.-C. Loison, F. Lique and J. Klos, *J. Phys. Chem. A* 2016, **120**, 2504−2513.

26. D. Husain and L. J. Kirsch, *Trans. Faraday Soc.* 1971, **67**, 2886−2895.

27. Willingham, C. B.; Taylor, W. J.; Pignocco, J. M.; Rossini, F. D. Vapor pressures and boiling points of some paraffin, alkylcyclopentane, alkylcyclohexane, and alkylbenzene hydrocarbons. Journal of Research of the National Bureau of Standards 1945, 35 (3), 219-244.

28. A. D. Becke, *J. Phys. Chem.* 1993, **98**, 5648.

29. P. J. Stephens, F. J. Devlin, C. F. Chablowski, M. J. Frisch, *J. Phys. Chem.* 1994, **98**, 11623.

30. T. H. Dunning Jr., *J. Chem. Phys.* 1989, **90**, 1007.

31. D. E. Woon, T. H. Dunning Jr., *J. Chem. Phys.* 1993, **98**, 1358.

32. R. A. Kendall, T. H. Dunning Jr., R. J. Harrison, *J. Chem. Phys.* 1992, **96**, 6796.

33. R. J. Bartlett, *Annu. Rev. Phys. Chem.* 1981, **32**, 359.

34. K. Raghavachari, G. W. Trucks, J. A. Pople, M. Head-Gordon, *Chem. Phys Lett.* 1989, **157**, 479.

35. J. Olsen, P. Jorgensen, H. Koch, A. Balkova, R. J. Bartlett, *J. Chem. Phys.* 1996, **104**, 8007.

36. C-H Chin, T. Zhu, J. Z. H. Zhang, *Phys. Chem. Chem*